




Analysis of macroscopic traffic flow model considering throttle dynamics

Wen Huan Ai^{1,a} , Ming Ming Wang^{1,b}, and Da Wei Liu^{2,c}

¹ College of Computer Science and Engineering, Northwest Normal University, Lanzhou 730070, Gansu, China

² College of Electrical Engineering, Lanzhou Institute of Technology, Lanzhou 730050, Gansu, China

Received 9 March 2023 / Accepted 29 May 2023 / Published online 25 June 2023

© The Author(s), under exclusive licence to EDP Sciences, SIF and Springer-Verlag GmbH Germany, part of Springer Nature 2023

Abstract. Due to the continuous development of economy and society, the pace of life is also accelerated, so people pay more and more attention to the time cost, and the transportation time cost is also a very important part of it. The traffic system is an important carrier to realize the traffic operation. The increase of automobile ownership requires the traffic system to be higher and higher. Moreover, vehicles in congested traffic flow inevitably start and stop operations with high frequency, which undoubtedly increases vehicle exhaust emissions, environmental pollution, noise pollution and other problems. For today's traffic system, vehicle dynamics information is also an important factor which affects the traffic system. Therefore, adding throttle, vehicle dynamics information, to the macro-traffic flow modeling research in this paper is a supplement and improvement to the current traffic flow theory research. By analyzing the equilibrium point, this paper proves the conditions for the existence of Hopf branch and saddle junction branch. Finally, numerical simulation is carried out, and the space–time diagram of density and phase plane are obtained through simulation, which can be used to describe the actual traffic phenomenon. Through numerical simulation, it is found that this model can better describe the congestion phenomenon of the actual traffic system, and provide scientific theoretical support for macroscopic traffic flow state analysis.

1 Introduction

With the acceleration of urbanization, daily travel has caused great pressure on the urban road traffic system, which eventually leads to more complex and crowded traffic flow. Traffic congestion will not only lead to accidents, but also aggravate environmental pollution, which is bound to have a negative impact on people's lives. To explore the intrinsic characteristics of traffic flow and the causes of traffic congestion, and take effective measures to curb it. It is necessary to develop more realistic traffic flow models, such as micro model [1–12] and macro model [13–19]. In addition, to reduce fuel costs and carbon emissions, researchers have developed fuel consumption models and emission models [20–22].

At present, complex nonlinear traffic phenomena have been the focus of research in recent years. Many traffic engineers, physicists and mathematicians have conducted in-depth nonlinear research on macroscopic traffic flow models. For traffic, a complex nonlinear system, the problem of traffic congestion can be essentially solved only by starting from its nonlinear nature.

Branch Analysis Method can describe and predict nonlinear traffic phenomena from the perspective of the global stability of the system, which will provide theoretical basis for fundamentally helping to solve traffic problems. In 1999, Yuji Igarashi et al. [23] studied the branch phenomenon of traffic flow based on the optimal velocity model proposed by Bando et al. [24]. Yuji Igarashi et al. proved the existence of Hopf branch in the model and described the traffic phenomenon. In 2010, Jin et al. [25] used the full-speed difference model to study the divergence problem, and carried out Hopf divergence analytic calculation on the model with Hopf theorem. In 2015, Ai et al. [26] proposed a branch analysis method based on macro-traffic flow model to describe and predict nonlinear traffic phenomena on highways from the perspective of global stability of the system, and obtained Hopf branch and saddle node branch of the model using this method. Then in 2018, Ge et al. carried out Hopf branch analysis and obtained Hopf branch points. The effects of delay time and velocity difference sensitivity in the model are discussed from Hopf branch. In 2021, Ge et al. [27, 28], based on the analysis of a micro traffic flow model, carried out Taylor expansion on the micro model to obtain the branch analysis of the macro model, and obtained the existence conditions and stability of the model Hopf branch.

^a e-mail: wenhuan618@163.com (corresponding author)

^b e-mail: 2537577724@qq.com

^c e-mail: liudawei20120901@163.com

Macro traffic flow modeling is also a method to describe traffic phenomena. Generally, macro-traffic flow modeling describes the behavioral evolution of traffic flow according to the relationship among traffic flow, average speed and average density in traffic flow. The research on macroscopic traffic flow model has been carried out for several decades, and many models have been proposed successively. The Fluid Dynamics Theory in the macroscopic model was proposed by Lighthill, Whitham and Richards [29, 30]. Therefore, in terms of macroscopic traffic flow modeling, current studies focus more on the mechanism of action and evolution characteristics of traffic flow, etc. Traditional macro-traffic flow models pay more attention to the average density, average speed, traffic flow and other vehicle state information and road structure information, etc. The impact factors are relatively simple, and the impact of throttle dynamics information on traffic flow evolution has not been considered at the macro level. Centering on the idea of macroscopic traffic flow modeling, this paper takes the influence of electronic throttle dynamics information [31, 32] on traffic flow evolution into consideration in macroscopic traffic flow modeling research.

In the field of macro-traffic flow modeling, most studies mainly consider the influence of factors such as vehicle state information and road structure information [33–35]. In the actual traffic system, vehicle dynamics information is also an important factor affecting the traffic system. Therefore, adding the vehicle dynamics information of throttle valve into the research of macroscopic traffic flow modeling is a supplement and perfection to the current research of traffic flow theory. The throttle dynamics information is added to the macroscopic traffic flow modeling. By considering the vehicle state information and throttle dynamics information at the same time, the evolution behavior of traffic flow is analyzed, and then the influence of throttle dynamics information on the evolution of traffic prevalence is analyzed. It has important research significance to provide scientific theoretical support for the macroscopic traffic flow state analysis.

2 Establishment of model

Electronic throttle is an important control component of vehicle engine, and electronic throttle system in the throttle opening accurate control is conducive to reducing vehicle exhaust emissions. It is worth mentioning that the more accurate throttle opening control, the more responsive the vehicle can meet the requirements of the public. Therefore, it is very necessary to add the dynamic information of electronic throttle into traffic flow modeling [36, 37].

We added throttle dynamics information into the research of macro-traffic flow modeling, and then carried out the design from the relationship model ET model of vehicle state information and vehicle dynamics information. ET model [38] was studied and proposed by Ioannou et al. which mainly described the

relationship between the dynamic information of electronic throttle and vehicle speed and acceleration. The driver can control the speed of the vehicle by controlling the opening of the electronic throttle valve. According to the ET model, at time t , the acceleration of car i can be expressed as:

$$a_i(t) = -b[v_i(t) - v_0] + c\bar{\theta}_i + d_i \quad (1)$$

Among it, $a_i(t)$ and $v_i(t)$ respectively represent the acceleration and speed of the number i car at time t , θ_i is the deviation for throttle, $\theta_i = \theta_i - \theta_0$, θ_0 is constant, v_0 is the vehicle speed in stable state, b and c changes over time, and d_i is the other perturbation not considered.

By analyzing the above ET model, the expression of electronic throttle deviation can be obtained, and then the expression of electronic throttle difference regarding vehicle speed and acceleration can be obtained:

$$\bar{\theta}_i = \{[a_i(t) + b(v_i(t) - v_0)] - d_i\}/c + \theta_0 \quad (2)$$

It follows that:

$$\Delta\theta_i = \theta_{i+1} - \theta_i = [a_{i+1}(t) - a_i(t) + b\Delta v_i(t)]/c \quad (3)$$

where the velocity difference $\Delta v_i(t) = v_{i+1}(t) - v_i(t)$. In addition, we know that the expression of T-FVD microscopic model [39–43] is:

$$a_i(t) = k[V(\Delta x_i(t)) - v_i(t)] + \lambda\Delta v_i(t) + \beta\Delta\theta_i \quad (4)$$

As the $V(\Delta x_i(t))$ is the best velocity function and position difference $\Delta x_i(t) = x_{i+1}(t) - x_i(t)$, $\beta > 0$, $k > 0$, $\lambda > 0$ is for sensitive coefficient.

Substituting Eq. (3) into Eq. (4) we can get a microscopic model that takes into account the throttle dynamics:

$$\begin{aligned} \frac{dv_n(t)}{dt} = & k[V(\Delta x_i(t)) - v_i(t)] + \lambda\Delta v_i(t) \\ & + k\{[a_{i+1}(t) - a_i(t) + b\Delta v_i(t)]/c\} \quad (5) \end{aligned}$$

Starting from the improved model, to obtain the corresponding macro-traffic flow model, a single discrete variable needs to be converted into a continuous variable. Specifically, first assume that the instantaneous speed of the $i + 1$ vehicle at the position x is equal to the average speed on the $[x - \frac{\Delta}{2}, x + \frac{\Delta}{2}]$ section, and the speed of the $[x - \frac{\Delta}{2}, x + \frac{\Delta}{2}]$ section depends on the average speed of the $[x + \frac{\Delta}{2}, x + \frac{3\Delta}{2}]$ section, where Δ corresponds to Δx in the microscopic traffic flow model, and changes with the spacing between different continuous vehicles.

From the connection between micro and macro, acceleration can be expressed as:

$$a_i(t) = \frac{du(x,t)}{dt} = \frac{\partial u(x,t)}{\partial x} \frac{\partial x}{\partial t} + \frac{\partial u(x,t)}{\partial t} = \frac{\partial u(x,t)}{\partial x} u(x,t) + \frac{\partial u(x,t)}{\partial t} \tag{6}$$

$$a_{i+1}(t) = \frac{du(x+\Delta,t)}{dt} = \frac{\partial u(x+\Delta,t)}{\partial x(x+\Delta)} \frac{\partial(x+\Delta)}{\partial t} + \frac{\partial u(x+\Delta,t)}{\partial t} = \frac{\partial u(x,t)}{\partial x} u(x+\Delta,t) + \frac{\partial u(x+\Delta,t)}{\partial t} \tag{7}$$

And there is

$$v_i(t) \rightarrow v(x,t), v_{i+1}(t) \rightarrow v(x+\Delta,t) \tag{8}$$

$$v(x+\Delta,t) = v(x,t) + \Delta v'_x(x,t) + \frac{1}{2} \Delta^2 v''_x \tag{9}$$

We bring this into the formula and ignore the non-linear term to get:

$$\frac{dv(x,t)}{dt} = \frac{1}{T}(v_e - v) + \left(\lambda + \frac{bk}{c}\right) \left(\Delta v'_x + \frac{1}{2} \Delta^2 v''_x\right) + kv''_x \Delta v \tag{10}$$

Organize the above equation as follows:

$$\frac{dv(x,t)}{dt} = \frac{1}{T}(v_e - v) + \left(\lambda \Delta + \frac{bk}{c} \Delta\right) v'_x + \left(\frac{\lambda}{2} \Delta^2 + \frac{bk}{2c} \Delta^2 + k \Delta v\right) v''_x \tag{11}$$

Expand the left side of the above equation as follows:

$$\frac{dv(x,t)}{dt} = \frac{\partial v(x,t)}{\partial t} + v \frac{\partial v}{\partial x} \tag{12}$$

Among them: $k = \lambda = \frac{1}{T}$, $\frac{\Delta}{T} = c0$, $\frac{\Delta^2}{2T} = \mu$

Combined with conservation equations, we can get new macroscopic traffic flow models

$$\begin{cases} \frac{\partial \rho}{\partial t} + \frac{\partial(\rho v)}{\partial x} = 0 \\ \frac{\partial v}{\partial t} + v \frac{\partial v}{\partial x} = \frac{1}{T}(v_e - v) + \left(\frac{b}{c} c_0 + c_0\right) \frac{\partial v}{\partial x} + \left(\mu + \frac{b}{c} \mu + c_0 v\right) \frac{\partial^2 v}{\partial x^2} \end{cases} \tag{13}$$

This model uses the periodic boundary condition, and the traffic phenomenon generated by the fulcrum is actually more obvious on the open loop section than the closed loop section, so this paper assumes that the

main road section is an open boundary condition, that is:

$$\rho(1,t) = \rho(2,t), \rho(L,t) = \rho(L-1,t), v(1,t) = v(2,t), v(L,t) = v(L-1,t)$$

Assume that model (13) has traveling-wave solution $\rho(z)$ and $v(z)$, in which $z = x - ct$ and traveling-wave velocity $c < 0$. Using the above results and substituting them into Eq. (13), we can obtain:

$$-c\rho_z + q_z = 0 \tag{14}$$

$$-c \frac{\partial v}{\partial z} + \left(v - \frac{b}{c} c_0 - c_0\right) \frac{\partial v}{\partial z} = \frac{1}{T} (V_e(\rho) - v) + \left(\mu + \frac{b}{c} \mu + c_0 v\right) \frac{\partial^2 v}{\partial z^2} \tag{15}$$

From the formula, we get:

$$q_z = c\rho_z \tag{16}$$

The derivative of $\rho v = q$ with respect to z at both ends of the equation yields:

$$q_z = \rho v_z + v \rho_z \tag{17}$$

Available from:

$$V_z = \frac{c\rho_z}{\rho} - \frac{q\rho_z}{\rho^2} \tag{18}$$

$$V_{zz} = \frac{c\rho - q}{\rho^2} \rho_{zz} \tag{19}$$

Meanwhile, in the formula, z is integrated, then:

$$-c\rho + q = const = q_* \tag{20}$$

At the same time, it obtains:

$$q = q_* + c\rho \tag{21}$$

So, bring it in, and after rewriting, you get:

$$\begin{aligned} &\left(v - c_1 - \frac{b}{c} c_0 + c_0\right) \left(\frac{c_1}{\rho} - \frac{q}{\rho^2}\right) \rho_z \\ &= \frac{1}{T} (V_e(\rho) - v) + \frac{c_1 \rho - q}{\rho^2} \left(\mu + \frac{b}{c} \mu + c_0 v\right) \rho_{zz} \end{aligned} \tag{22}$$

Simplification yields about second-order ordinary differential equations:

$$\rho_{zz} - G(\rho, q_*) \rho_z - F(\rho, c, q_*) = 0 \tag{23}$$

Among it:

$$G(\rho, q_*) = \frac{c q_* + 2c_1 c \rho + c_0 \rho (b+c)}{\rho \mu (c-b) + c c_0 (q_* + c_1 \rho)} \tag{24}$$

Table 1 Types of equilibrium points and their stability when it gives model parameters

(c, q_*)	ρ_1	ρ_2	ρ_3
$(-1.371, 0.2)$	0.0065 $F'_i > 0$, saddle point Unstable for $z \rightarrow \pm \infty$	0.0938 $\Delta_i < 0, G_i < 0$, spiral point Stable for $z \rightarrow +\infty$ Unstable for $z \rightarrow -\infty$	0.1447 $F'_i > 0$, saddle point Unstable for $z \rightarrow \pm \infty$
$(-1.38, 0.64)$	0.0223 $F'_i > 0$, saddle point Unstable for $z \rightarrow \pm \infty$	0.0594 $\Delta_i < 0, G_i < 0$, spiral point Stable for $z \rightarrow +\infty$ Unstable for $z \rightarrow -\infty$	

$$F(\rho, c, q_*) = \frac{\rho V_e(\rho) - q_* - c_1 \rho}{T q_*} * \frac{\rho^2 c}{(\rho \mu (c-b) + c c_0 (q_* + c_1 \rho))} \tag{25}$$

Let $y = \frac{d\rho}{dz}$, Eq. (1) can be converted to a system of first-order ordinary differential equations:

$$\begin{cases} \frac{d\rho}{dz} = y \\ \frac{dy}{dz} = G(\rho, q_*)y + F(\rho, c, q_*) \end{cases} \tag{26}$$

Then, for the type of equilibrium point and its stability, it is mainly determined from the equations formed by Eq. (26), let the right end of Eq. (26) is 0, it is known that $y = 0$ and $F = 0$, the equilibrium point coordinate $(\rho_i, 0)$ can be obtained. Then, according to the equilibrium point coordinates, the Eq. (26) is expanded by Taylor, and the linear representation of the system can be obtained:

$$\begin{cases} \rho' = y \\ y' = G(\rho_i, q_*)y + F'(\rho_i, c, q_*)(\rho - \rho_i) \end{cases} \tag{27}$$

Thus, the Jacobian matrix of the system at the equilibrium point can be written:

$$L = \begin{bmatrix} 0 & 1 \\ F'_i & G_i \end{bmatrix} \tag{28}$$

The corresponding characteristic equation is:

$$\lambda^2 - G_i \lambda - F'_i = 0 \tag{29}$$

where $G_i(\rho_i, c, q_*) = G(\rho, c, q_*)$, $F' = F'(\rho, c, q_*)$ is obtained:

$$G_i = \frac{c q_* + 2 c_1 c \rho_i + c_0 \rho_i (b + c)}{\rho_i \mu (c - b) + c c_0 (q_* + c_1 \rho_i)} \tag{30}$$

$$F'_i = \frac{1}{T q_*} \frac{(3 \rho_i^2 c V_e(\rho_i) + c V'_e(\rho_i) - 2 \rho_i c q_* - 2 \rho_i c c_1)(\rho_i \mu (c - b) + c c_0 (q_* + c_1 \rho_i)) - (\rho_i^3 c V_e(\rho_i) - \rho_i^2 c q_* - c c_1 \rho_i^2)(\mu (c - b) + c c_0 c_1)}{(\rho_i \mu (c - b) + c c_0 (q_* + c_1 \rho_i))^2} \tag{31}$$

Because at the equilibrium point $(\rho_i, 0)$, $F = 0$, then $\rho_i V_e(\rho) - q_* - c_1 \rho_i = 0$, according to the qualitative theory of differential equation, it can determine the linear

system (26) the type of equilibrium point is as follows: (a) when $F'_i > 0$, the equilibrium point is the saddle point; (b) When $G_i^2 + 4F'_i > 0$ and $F'_i < 0$, the equilibrium is the node; (c) When $G_i^2 + 4F'_i < 0$ and $G_i \neq 0$, the equilibrium point is the focus; (d) When $F'_i < 0$ and $G_i = 0$, the equilibrium is centered. When $z \rightarrow \pm\infty$, the stability of linear systems at saddle points is unstable. When $G_i < 0$ (or $G_i > 0$), the stability at nodes and focal points is stable for $z \rightarrow +\infty$ (or $z \rightarrow -\infty$).

According to Hartman-Grossman linearization theory, nonlinear system (26) and linear system (27) have the same equilibrium point. For the equilibrium point that is not the center, the stability case at the equilibrium point, the nonlinear system (26) and the linear system (27) are consistent. Given the values of any set of traveling-wave velocity c and traveling-wave parameter q_* , the equilibrium ρ_1, ρ_2, ρ_3 of the linear system (26) can be solved. The equilibrium velocity function proposed in literature [44] is selected as follows:

$$V_e[\rho] = v_f \left\{ \left[1 + \exp\left(\frac{\rho}{0.06} - 0.25\right) \right]^{-1} - 3.72 \times 10^{-6} \right\} \tag{32}$$

Here, v_f represents the free flow velocity and ρ_m represents the maximum or congestion density.

The values of parameters in the model in this chapter are as follows: $v_f = 30$ m/s, $\rho_m = 0.2$ veh/m, $T = 10$ s, $c_0 = 11$ m/s, $\mu = 550$. When ρ equals 0, this is a trivial equilibrium point, and it has no practical significance, so this paper only needs to discuss other equilibrium points. Based on the above discussion and Eq. (31), the type and stability of the equilibrium point can be determined, as shown in Table 1, where the equilibrium point is indicated by $\rho_i (i = 1, 2, 3)$.

The two sets of parameters in Table 1 were selected to numerically simulate the stability at the equilibrium point of the nonlinear system (26).

Figure 1 corresponds to the first scenario in Table 1. It can be seen from Table 1 that when $z \rightarrow \pm\infty$, the system is unstable at the equilibrium point $(\rho_1, 0)$ and $(\rho_3, 0)$, and the nearby rails are far away from the point. As $z \rightarrow +\infty$, there are several helical rails close to the saddle point $(\rho_1, 0)$ tend to focus $(\rho_2, 0)$, and because of the influence of the nearby saddle point $(\rho_3, 0)$, the

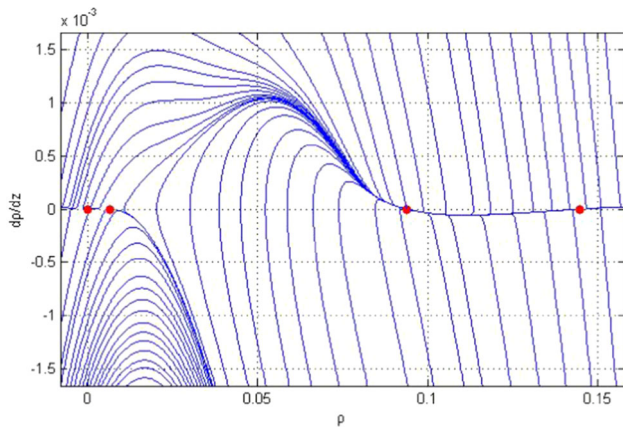


Fig. 1 Phase ρ - y planar track diagram with traveling-wave velocity $c = -1.371$, traveling-wave parameters $q_* = 0.2$

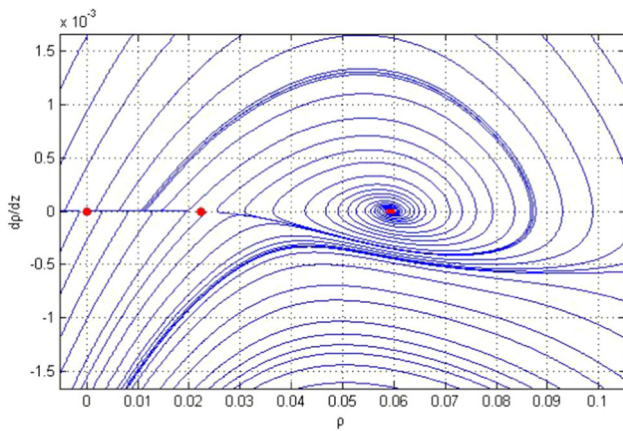


Fig. 2 Phase ρ - y planar track diagram with traveling-wave velocity $c = -1.38$ traveling-wave parameters $q_* = 0.64$

helical state of the rails tend to focus is not obvious. As z goes to $z \rightarrow -\infty$, the orbitals move away from the focus and eventually approach infinity. It is shown that the system is stable at $(\rho_2, 0)$ when $z \rightarrow +\infty$. As z goes to $z \rightarrow -\infty$, these orbitals move away from the focus and eventually approach infinity. These orbitals can be regarded as the saddle-focal-saddle point solution of the system. It is shown that the system is stable at the equilibrium point $(\rho_2, 0)$ when $z \rightarrow +\infty$ and unstable at the equilibrium point $(\rho_2, 0)$ when $z \rightarrow -\infty$.

Figure 2 corresponds to the second scenario in Table 1. Figure 2 also shows that the system is unstable at the equilibrium point $(\rho_1, 0)$. The spiral triggered near $(0.05, 0)$ tends to focus $(\rho_2, 0)$ when $z \rightarrow +\infty$, and the

system is stable at this point; As $z \rightarrow -\infty$, away from the focus $(\rho_2, 0)$, the system is unstable.

The overall structure of multiple equilibrium points interacting with each other can be clearly seen from the two-phase planar graph, and the influence of the equilibrium point on the curve trajectories around the equilibrium point can be seen from the changes of the curve trajectories around the equilibrium point, which is consistent with the analysis results.

3 Hopf branching conditions for the model

Lemma 1 [45] Consider the system $\dot{x} = f(x, \lambda), x \in R^n, \lambda \in R, \lambda$ as a variadic parameter. If (x_0, λ) the equilibrium condition is satisfied, $f(x, \lambda)|_{(x_0, \lambda_0)} = 0_{n \times 1}$, it is noted $L = D_x f(x, \lambda)|_{(x_0, \lambda_0)}$ that its eigenvalue is, $\alpha(\lambda) \pm i\beta(\lambda)$ and if $\alpha(\lambda_0) = 0$ and $\beta(\lambda_0) = \omega > 0$, then the system has $c = a(\lambda)|_{\lambda_0} \neq 0$ Hopf branch $\lambda = \lambda_0$ at the place.

For the system (26) let q_* be a variable parameter, it for all q_* equilibrium point $(\rho_0, 0)$, the derivative matrix $L(q_*)$ out of the equilibrium point is also the Jacobian matrix of the system at the equilibrium point, as shown below:

$$L(q_*) = \begin{pmatrix} 0 & 1 \\ F(\rho, c, q_*) & G(\rho, q_*) \end{pmatrix} \Big|_{\substack{\rho = \rho_0 \\ q_* = q_*_0}} \triangleq \begin{pmatrix} A_1 & A_2 \\ A_3 & A_4 \end{pmatrix} \tag{33}$$

Among it:

$$G(\rho, q_*) = \frac{cq_* + 2c_1c\rho + c_0\rho(b+c)}{\rho\mu(c-b) + cc_0(q_* + c_1\rho)} \tag{34}$$

$$F(\rho, c, q_*) = \frac{\rho V'_c(\rho) - q_* - c_1\rho}{T} * \frac{\rho^2 c}{(\rho\mu(c-b) + cc_0(q_* + c_1\rho))q_*} \tag{35}$$

Let its eigenvalue be λ , $\lambda = \alpha(q_*) \pm j\beta(q_*)$ then its eigenequation is:

$$\lambda^2 - (A_1 + A_4)\lambda + (A_1A_4 - A_2A_3) = 0 \tag{36}$$

The equation has a pair of complex eigenvalues $\alpha(q_*) \pm j\beta(q_*)$ then:

$$\alpha(q_*) = \frac{A_1 + A_4}{2} = \frac{1}{2} \left(\frac{cq_* + 2c_1c\rho + c_0\rho(b+c)}{\rho\mu(c-b) + cc_0(q_* + c_1\rho)} \right) \tag{37}$$

$$\beta(q_*) = \sqrt{(A_1A_4 - A_2A_3) - \frac{(A_1 + A_4)^2}{4}} \tag{38}$$

$$= \sqrt{-\frac{\rho V_e'(\rho) - q_* - c_1\rho}{T} * \frac{\rho^2c}{(\rho\mu c - b\rho\mu + cc_0(q_* + c_1\rho))q_*} - \frac{1}{4} \left(\frac{cq_* + 2c_1c\rho + c_0\rho(b+c)}{\rho\mu(c-b) + cc_0(q_* + c_1\rho)} \right)^2}$$

$$c = \dot{\alpha}(q_*)_{q_*} = \frac{1}{2} \frac{(\rho\mu c - b\rho\mu)c - (c_1c\rho + c_0b\rho + c_0c\rho)cc_0}{(\rho\mu(c-b) + cc_0(q_* + c_1\rho))^2} \neq 0 \tag{39}$$

$$\begin{cases} x'_1 = \alpha(\gamma)x_1 - \omega(\gamma)x_2 + \tilde{f}_1(x_1, x_2, \gamma) \\ x'_2 = \omega(\gamma)x_1 + \alpha(\gamma)x_2 + \tilde{f}_2(x_1, x_2, \gamma) \end{cases} \tag{44}$$

Cause $\alpha(\rho_0, q_{*0}) = 0$, namely:

$$\alpha(\rho_0, q_*) = \frac{1}{2} \left(\frac{q_*c + 2c_1c\rho_0 + c_0\rho_0(b+c)}{\rho_0\mu c - b\rho_0\mu + cc_0(q_* + c_1\rho_0)} \right) |_{q_* = q_{*0}} \approx 0 \tag{40}$$

From this, we get:

$$q_{*0} = -\frac{2c_1c\rho_0 + c_0\rho_0(b+c)}{c} \tag{41}$$

At the same time,

$$\beta(\rho_0, q_{*0}) = \sqrt{-\frac{\rho V_e'(\rho) - q_* - c_1\rho}{T} * \frac{\rho^2c}{(\rho\mu c - b\rho\mu + cc_0(q_* + c_1\rho))q_*}} \tag{42}$$

$$\begin{cases} \rho = \rho_0 \\ q_* = q_{*0} \end{cases}$$

Because the $V_e'(\rho) < 0$, so when $-\rho^2V_e'(\rho_0) > q_{*0} > 0\beta(\rho_0, q_{*0}) > 0$. In this case, the system has Hopf branch at $q_* = q_{*0}$.

4 Hopf branch types for models

For Hopf branch problem, since N -dimensional systems can be restricted to two-dimensional central manifolds by the central manifold method, only Hopf branch of two-dimensional systems is considered.

Lemma 2 [45]: *Set up a two-dimensional system with parameters*

$$x' = f(x, \gamma), x = (x_1, x_2)^T \in R^2, \gamma \in R \tag{43}$$

The equilibrium point of is the origin $O(0, 0)$, and the eigenvalues at the origin are $\alpha(\gamma) \pm i\omega(\gamma)$. At that time, $\gamma = 0$ the partial derivative matrix of the system has a pure virtual eigenvalue, $i\omega_0$ that is $\alpha(0) = 0, \omega(0) = \omega_0 > 0$. By means of coordinating transformation, the system (43) can be written as

where $\tilde{f}_1, \tilde{f}_2 = O(x_1^2 + x_2^2)$.

Theorem 1 (ODE's Hopf branching theorem) *Let the partial matrix at the re-origin of the system (Eq 43) have eigenvalues $D(\gamma)$ and satisfy $\alpha(\gamma) \pm i\omega(\gamma)$ the sum $\alpha(0) = 0, \omega(0) = \omega_0 > 0$, then there is an analytic function $c = \alpha'(0) \neq 0$*

$$\gamma(\varepsilon) = \sum_{k=0}^{\infty} \gamma_k \varepsilon^k \tag{45}$$

Such that $\gamma = \gamma(\varepsilon) \neq 0$ for the pair, the system (42) has a unique closed orbit within the sufficiently small neighborhood of the origin of Γ_ε its period

$$T(\varepsilon) = \frac{2\pi}{\omega_0} \left(1 + \sum_{k=0}^{\infty} \gamma_k \varepsilon^k \right) \tag{46}$$

When $\varepsilon \rightarrow 0, \gamma(\varepsilon) \rightarrow 0$ comes, Γ_ε tends to the origin. γ_{k1} is denoted as the first coefficient in expansion Eq. (45) that is not equal to zero. Γ_ε is a stable limit ring when γ_{k1} is the same sign with c , Γ_ε is an unstable limit when γ_{k1} is different with sign.

Literature [46] gives a proof of theorem one and the equations for calculating the coefficients γ_{k1}, τ_k , especially when $k = 2$,

$$\gamma_2 = -\frac{a}{c}, \tau_2 = -\frac{b + \gamma_2\omega'(0)}{\omega_0} \tag{47}$$

Among them, the first Lyapunov index of the system can be calculated as follows:

$$a = \left(\frac{1}{16} \right) \left[\tilde{f}_{1xxx} + \tilde{f}_{1xyy} + \tilde{f}_{2xxy} + \tilde{f}_{2yyy} \right] + \left(\frac{1}{16\omega_0} \right) \left[\tilde{f}_{1xy} (\tilde{f}_{1xx} + \tilde{f}_{1yy}) - \tilde{f}_{2xy} (\tilde{f}_{2xx} + \tilde{f}_{2yy}) - \tilde{f}_{1xx}\tilde{f}_{2yy} + \tilde{f}_{1yy}\tilde{f}_{2xy} \right] \tag{48}$$

where $\tilde{f}_{1xxx}, \tilde{f}_{2xxx}$ etc. are the partial derivative at $\tilde{f}_1, \tilde{f}_2 (0, 0, 0)$. Here, a is an important parameter for judging the stability of the limit ring, assuming that the theorem condition is true, according to the Hopf branch, there are the following stability conclusions:

If $a < 0 (> 0)$. then the limit ring Γ_ε is stable (unstable). If a is different (same) sign with the c , the Hopf branch is supercritical (subcritical); If $a = 0$ so, the Hopf branch is degenerate.

For system (26), set q_* as variable parameter, It has an equilibrium $(\rho_0, 0)$ for everything q_* , make $\tilde{\rho} = \rho - \rho_0$ coordinate translation, the equilibrium point moves to the origin, then the system can be expressed as follows:

$$\begin{cases} \tilde{\rho}' = y, \\ y' = \tilde{G}(\tilde{\rho}, q_*)y + \tilde{F}(\tilde{\rho}, c, q_*). \end{cases} \tag{49}$$

By $(\tilde{\rho}, y) = (0, 0)$ performing a Taylor unfolding at the equilibrium point, the system can be linearized to:

$$\tilde{x}' = L(q_*)\tilde{x} + f \tag{50}$$

where f is a smooth vector function whose constituent elements $f_{1,2}$ are the Taylor expansion of the least quadratic term with respect to \tilde{x} , which can be expressed as follows:

$$f = \begin{bmatrix} 0 \\ k_{11}\tilde{\rho}^2 + k_{22}y^2 + k_{12}\tilde{\rho}y + k_{111}y^3 + k_{112}\tilde{\rho}^2y \\ + k_{122}\tilde{\rho}y^2 + O(\tilde{\rho}, y)^4 \end{bmatrix} \tag{51}$$

The Jacobi matrix $L(q_*)$ can be expressed as follows:

$$L(q_*) = \begin{pmatrix} 0 & 1 \\ \frac{\rho V'_e(\rho) - q_* - c_1\rho}{T^2 c} & \frac{cq_* + 2c_1c\rho + c_0\rho(b+c)}{\rho\mu(c-b) + cc_0(q_* + c_1\rho)} \end{pmatrix} = \begin{pmatrix} 0 & 1 \\ b(q_*) & d(q_*) \end{pmatrix} \tag{52}$$

Its eigenvalues are the root of the following characteristic equation:

$$\lambda^2 - \sigma\lambda + \Delta = 0 \tag{53}$$

thereinto, $\sigma = \sigma(q_*) = d(q_*) = trL(q_*)$, $\Delta = \Delta(q_*) = -b(q_*) = detL(q_*)$,

$$\lambda_{1,2}(q_*) = \frac{1}{2}(\sigma(q_*) \pm \sqrt{\sigma^2(q_*) - 4\Delta(q_*)}) \tag{54}$$

Obtained by the Hopf branching condition:

$$\sigma(0) = 0, \Delta(0) = \omega_0^2 > 0 \tag{55}$$

For smaller $|q_*|$ ingestible variables:

$$\alpha(q_*) = \frac{1}{2}\sigma(q_*), \omega(q_*) = \frac{1}{2}\sqrt{4\Delta(q_*) - \sigma^2(q_*)} \tag{56}$$

This results in the following eigenvalue expression:

$$\lambda_1(q_*) = \lambda(q_*), \lambda_2(q_*) = \bar{\lambda}(q_*) \tag{57}$$

Thereinto:

$$\lambda(q_*) = \alpha(q_*) + i\omega(q_*), \alpha(0) = 0, \omega(0) = \omega_0 > 0 \tag{58}$$

Let $\omega_{re} + i\omega_{im}$ be the eigenvector of $L(q_*)$ corresponding to the eigenvalue $\lambda(q_*)$, and have:

$$L(\omega_{re} + i\omega_{im}) = i\omega_0(\omega_{re} + i\omega_{im}) \tag{59}$$

Considering that the real and imaginary parts on both sides of the above equation equal sign are equal, we get:

$$\begin{cases} L\omega_{im} = \omega_0\omega_{re} \\ L\omega_{re} = -\omega_0\omega_{im} \end{cases} \tag{60}$$

The collation Eq. (60) is as follows:

$$L[\omega_{im} \ \omega_{re}] = [\omega_{im} \ \omega_{re}] \begin{bmatrix} 0 & -\omega_0 \\ \omega_0 & 0 \end{bmatrix} \tag{61}$$

From this:

$$[\omega_{im} \ \omega_{re}]^{-1}L[\omega_{im} \ \omega_{re}] = \begin{bmatrix} 0 & -\omega_0 \\ \omega_0 & 0 \end{bmatrix} \tag{62}$$

Cause:

$$\tilde{y} = [\omega_{im} \ \omega_{re}]^{-1}\tilde{x} \tag{63}$$

Namely:

$$\tilde{y}' = [\omega_{im} \ \omega_{re}]^{-1}\tilde{x}' \tag{64}$$

Bringing Eq. (50) into Eq. (64) yields:

$$\begin{aligned} \tilde{y}' &= [\omega_{im} \ \omega_{re}]^{-1}L[\omega_{im} \ \omega_{re}]\tilde{y} + [\omega_{im} \ \omega_{re}]^{-1}f \\ &= \begin{bmatrix} 0 & -\omega_0 \\ \omega_0 & 0 \end{bmatrix}\tilde{y} + [\omega_{im} \ \omega_{re}]^{-1}f \end{aligned} \tag{65}$$

In addition, $L(q_*)$ the eigenvectors can be calculated as follows:

$$\omega_{re} + i\omega_{im} = \begin{bmatrix} 0 \\ 1 \end{bmatrix} + i \begin{bmatrix} -\frac{1}{\sqrt{-b(q_*)}} \\ 0 \end{bmatrix} \tag{66}$$

Bringing the values of Eq. (51) and sum into equation $\omega_{im}(\omega_{re})$ yields:

$$\tilde{y}' = \begin{bmatrix} 0 & -\omega_0 \\ \omega_0 & 0 \end{bmatrix} \tilde{y} + \begin{bmatrix} 0 \\ k_{111}\tilde{\rho}^2 + k_{222}y^2 + k_{112}\tilde{\rho}y + k_{111}y^3 \\ +k_{1112}\tilde{\rho}^2y + k_{1122}\tilde{\rho}y^2 + O(\tilde{\rho}, y)^4 \end{bmatrix} \tag{67}$$

Equation (67) is in the same form as Eq. (44), so according to Eq. (48), the system (26) can a be calculated as follows:

$$a = \left(\frac{1}{16}\right) \left[\tilde{f}_{2\tilde{y}_1\tilde{y}_1\tilde{y}_2} + \tilde{f}_{2\tilde{y}_2\tilde{y}_2\tilde{y}_2} \right] + \left(\frac{1}{16\omega_0}\right) \left[-\tilde{f}_{2\tilde{y}_1\tilde{y}_2} \left(\tilde{f}_{2\tilde{y}_1\tilde{y}_1} + \tilde{f}_{2\tilde{y}_2\tilde{y}_2} \right) \right] \tag{68}$$

Further, the value of c can be calculated as follows:

$$c = \alpha'(q_*) = \frac{1}{2} \left(\frac{cq_* + 2c_1c\rho + c_0\rho(b+c)}{\rho\mu(c-b) + cc_0(q_* + c_1\rho)} \right) |_{q_* = 0} > 0 \tag{69}$$

Therefore, for the system (26), the Hopf branch is supercritical when $a < 0$ and subcritical when $a > 0$.

5 Saddle branching conditions for the model

Lemma 3 [45]: Consider the system $x' = f(x, \lambda), x \in R^n, \lambda \in R, \lambda$ is a variable parameter. If (x_0, λ) satisfies the equilibrium condition $f(x, \lambda)|(x_0, \lambda_0) = 0_{n \times 1}$, note $L = D_x f(x, \lambda)|(x_0, \lambda_0)$, make Ψ and Φ L about unit characteristic vectors, respectively, namely $\Psi L = 0$ and $L\Phi = 0$, is when the following conditions to satisfy, $\lambda = \lambda_0$ is saddle section branch of the system.

$$(i) a = \Psi \frac{\partial}{\partial q_*} f(x, \lambda) |_{(x_0, \lambda_0)} \neq 0 \tag{70}$$

$$(ii) b = \Psi \cdot \sum_{i=1}^n e_i \left[\Phi^T \frac{\partial^2}{\partial x^2} f_i(x, \lambda) |_{(x_0, \lambda_0)} \Phi \right] \neq 0 \tag{71}$$

Is for any small $\varepsilon > 0$, the solution of curve near (x_0, λ_0) , approximate expression for:

$$x = \varepsilon\Phi + o(\varepsilon^2), \lambda = \frac{\varepsilon^2 b}{2a} + o(\varepsilon^3). \tag{72}$$

For system (26), set q_* to variable parameters, the matrix of derivatives at the equilibrium point is shown in Eq. (33). When $q_* = -\rho^2 V_e'(\rho)$ there is $\Phi = \begin{pmatrix} 1 \\ 0 \end{pmatrix}$ satisfaction $L\Phi = 0$.

At this point,

$$\Psi L = 0 \Rightarrow \Psi = \left(\frac{cq_* + 2c_1c\rho + c_0\rho(b+c)}{\rho\mu(c-b) + cc_0(q_* + c_1\rho)} \ 1 \right) \tag{73}$$

Substituting the variables Ψ and Φ into Eqs. (70) and (71) gives:

$$\begin{aligned} a &= \Psi \frac{\partial}{\partial q_*} f(x, q_*) |_{(x_0, q_{*0})} \\ &= \left(\frac{cq_* + 2c_1c\rho + c_0\rho(b+c)}{\rho\mu(c-b) + cc_0(q_* + c_1\rho)} \ 1 \right) \left(\frac{0}{-\frac{\rho^2 c}{T(\rho\mu(c-b) + cc_0(q_* + c_1\rho))}} \right) \\ &= - \frac{\rho^2 c}{T(\rho\mu(c-b) + cc_0(q_* + c_1\rho))} \neq 0 \tag{74} \\ b &= \Psi \sum_{i=1}^n e_i \left[\Phi^T \frac{\partial^2}{\partial x^2} f_1(x, \lambda) |_{(x_0, \lambda_0)} \Phi \right] \\ &= \left(\frac{cq_* + 2c_1c\rho + c_0\rho(b+c)}{\rho\mu(c-b) + cc_0(q_* + c_1\rho)} \ 1 \right) \cdot \begin{pmatrix} \begin{bmatrix} 1 & 0 \\ 0 & 0 \end{bmatrix} \begin{bmatrix} 1 \\ 0 \end{bmatrix} \\ \begin{bmatrix} 1 & 0 \\ 0 & 0 \end{bmatrix} \begin{bmatrix} Z & L \\ L & 0 \end{bmatrix} \begin{bmatrix} 1 \\ 0 \end{bmatrix} \end{pmatrix} \\ &= \frac{cc_0(q_* + c_1\rho)^2 + cV_e'(\rho) - 2\rho_0cq_* - 2c_1c\rho_0(\rho_0\mu(c-b)) + (3\rho_0^3cV_e(\rho) + cV_e'(\rho) - 2\rho_0cq_* - 2c_1c\rho_0)(\mu(c-b) + cc_0c_1) + cc_0(q_* + c_1\rho) - (\rho_0^3cV_e(\rho) - \rho_0^2cq_* - c_1c\rho_0^2)(\mu(c-b) + cc_0c_1) - 2(\rho_0\mu(c-b) + cc_0(q_* + c_1\rho_0))(\mu(c-b) + cc_0c_1)(3\rho_0^2cV_e(\rho) + ((3\rho_0^2cV_e'(\rho) + 6\rho_0cV_e(\rho) + cV_e''(\rho) - 2cq_* - 2c_1c_1)\rho_0\mu(c-b) + cc_0(q_* + c_1\rho_0)) - (3\rho_0^2cV_e(\rho) + \rho_0^3cV_e'(\rho) - 2\rho_0cq_* - 2c_1c\rho_0))(\mu(c-b) + cc_0c_1)(\rho_0\mu(c-b))}{(\rho\mu(c-b) + cc_0(q_* + c_1\rho))^4} \neq 0 \tag{75} \end{aligned}$$

Thereinto

$$\begin{aligned} Z(\rho_i, c, q_*) &= cc_0(q_* + c_1\rho) + cc_0(q_* + c_1\rho)^2 \\ &\quad - (\rho_0^3cV_e(\rho) - \rho_0^2cq_* - c_1c\rho_0^2)(\mu(c-b) + cc_0c_1) \\ &\quad - 2(\rho\mu(c-b) + cc_0(q_* + c_1\rho))(\mu(c-b) + cc_0c_1) \\ &\quad + (3\rho_0^2cV_e(\rho) + (3\rho_0^2cV_e(\rho) + cV_e'(\rho) - 2\rho_0cq_* - 2c_1c\rho)(\mu(c-b) + cc_0c_1) \\ &\quad + ((3\rho_0^2cV_e'(\rho) + 6\rho_0cV_e(\rho) + cV_e''(\rho) - 2cq_* - 2c_1c_1)\rho\mu(c-b) + cc_0(q_* + c_1\rho_0))^2 + cV_e'(\rho) \\ &\quad - 2\rho_0cq_* - 2c_1c\rho)(\rho_0\mu(c-b) + cc_0(q_* + c_1\rho)) \\ &\quad - (3\rho_0^2cV_e(\rho) + \rho_0^3cV_e'(\rho) - 2\rho_0cq_* - 2c_1c\rho)(\rho_0\mu(c-b) + cc_0(q_* + c_1\rho)) \\ &= \frac{(\rho_0) - 2\rho_0cq_* - 2c_1c\rho)(\mu(c-b) + cc_0c_1)(\rho\mu(c-b))}{(\rho\mu(c-b) + cc_0(q_* + c_1\rho))^4} \tag{76} \end{aligned}$$

And

$$L(\rho_i, c, q_*) = \frac{(2c_1c + c_0(b+c))(\rho\mu(c-b) + cc_0(q_* + c_1\rho)) - (cq_* + 2c_1c\rho + c_0\rho(b+c))(\mu(c-b) + cc_0c_1)}{(\rho\mu(c-b) + cc_0(q_* + c_1\rho))^4} \tag{77}$$

So when the $q_{*0} = -\rho_0^2 V_e'(\rho_0)$ system (26) exists in $q^* = q_{*0}^*$ the saddle branch.

6 Numerical simulation

First, to verify that our newly proposed model can reproduce the stop-and-go phenomenon of real traffic flow under different initial densities, we choose different initial densities to simulate the density space–time diagram. The figure shows the spatio-temporal plot of density when the initial density is $0.01\text{veh/m} < \rho_0 < 0.09\text{veh/m}$.

The numerical results under different initial densities are shown in the figure. According to the figure, we find that the traffic condition will be unstable when the initial density is $0.01\frac{\text{veh}}{\text{m}} < \rho_0 < 0.09\text{veh/m}$.

Under the given initial boundary conditions mentioned above, the following conclusions can be drawn according to the simulation diagram of the density waveform of the new model shown in Fig. 3a–f:

- (1) As can be seen from Fig. 3a–f, when the initial density value is small, the new model can eliminate the external disturbance well, as shown in Fig. 3a, b. However, with the increase of the initial density, the traffic flow gradually becomes less stable, and the disturbance does not decrease with the passage of time, but produces greater fluctuations, as shown in Fig. 3c–e. When the initial density continues to increase, the initial density value reaches the stable interval of the macroscopic traffic flow model. The disturbance wave of the density space–time diagram gradually disappears, eliminating external interference, and the traffic flow gradually returns to a stable state, as shown in Fig. 3f.
- (2) As shown in Fig. 3c–e, within a certain range, with the increase of the initial density, the disturbance does not decrease, but instead as time goes on, multiple aggregation waves as shown in Fig. 3c, multiple disturbance waves as shown in Fig. 3d, and an increase in disturbance as shown in Fig. 3e are generated. When the traffic flow density is lower than the critical density, the small disturbance will dissipate quickly and evolve into a uniform flow. When the initial density increases to $\rho_0 = 0.04586\text{veh/m}$, a complex local structure consisting of two or more clusters is formed. Therefore, the local clustering phenomenon of traffic flow is reproduced in Fig. 3c, and the actual traffic state will eventually appear congestion. However, when the initial density continues to increase, as shown in Fig. 3f, the disturbance gradually disappears and the traffic flow gradually returns to a stable state as time goes by. In summary, through numerical simulation, the stable state of traffic flow described by the macro model proposed in this paper is observed, and its boundary stability conditions are obtained. When the initial density $\rho_0 > 0.09\text{veh/m}$, or $\rho_0 < 0.01\text{veh/m}$, the disturbance in the traffic flow will not be amplified; When ρ_0 is not in the stable condition area, the disturbance will be amplified,

and even appear local cluster effect, stop-and-go vehicle phenomenon.

- (3) As shown in the Fig. 3g–j, 3g, i are the density space–time diagram of macro model considering throttle information, Fig. 3h, j are the density space–time diagram of FVD macro model. We find that under the same parameter conditions, as the density decreases or increases, the small perturbations develop into single clusters and multiple clusters; under the same initial density ρ , the influence of throttle opening angle can effectively suppress traffic congestion.

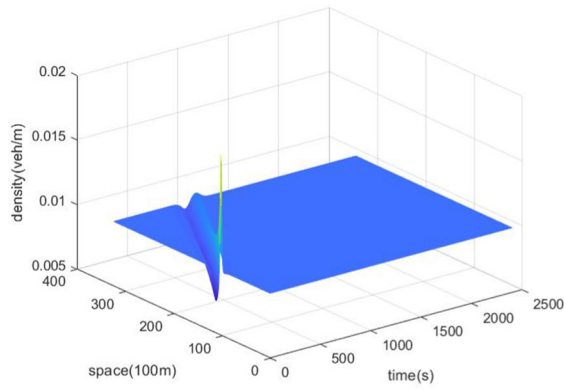
According to the simulation results of the FVD macro model and the throttle macro model, the following conclusions can be drawn: whether the traffic flow is in a stable state (Fig. 3i, j) or an unstable state (Fig. 3g, h), under the same initial density conditions, the fluctuation of the density waveform of the macro model considering the throttle is smaller than that of the FVD macro model when the disturbance diverges or the disturbance disappears. Therefore, it can be concluded that the macroscopic traffic flow model considering the influence of electronic throttle dynamics can effectively curb traffic congestion. The stability, anti-interference ability and ability to eliminate external disturbances of the new macro model are stronger than those of the FVD macro model without considering the throttle dynamics information, which further verifies the effectiveness of the new model.

Next, we choose different equilibrium points as starting points to study various branch of nonlinear systems (26). In the beginning, we use the above equilibrium point as an example to plot the following figure, where the parameters are selected as variable parameters with an initial value of 0.2. You can find three special points in this range which respectively are a Hopf branch point (H) and two limiting branch points (LP), as shown in Fig. 4.

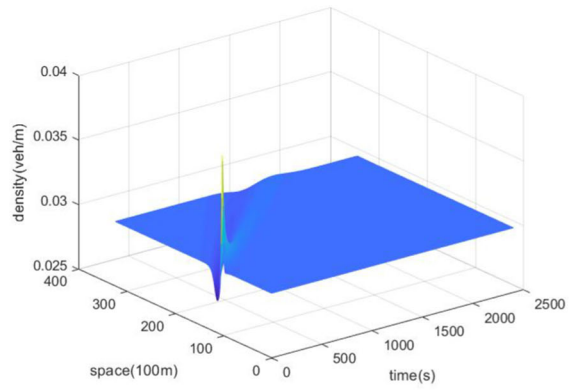
When q_* is 0.817848, the state variables for Hopf branch point is (0.050047,0), at this time, the vehicle density is $\rho_0 = 0.050047\text{eh/m}$, and two eigenvalues were $4.4729\text{e}-08 + 0.019825i$ and $4.4729\text{e}-08 - 0.019825i$. The real part of a pair of conjugate eigenvalues is considered to be 0, which is the sign of judging it as a Hopf branch, and its maximum lyapunov exponent is $5.555356\text{e} + 01$.

The first limit branch occurs when the variable parameter is 0.891695. The state variables is (0.040665,0), the corresponding vehicle density is $\rho_0 = 0.040665\text{eh/m}$. The eigenvalues were $-1.8044\text{e}-05$ and 0.018863 , respectively. Obviously the previous eigenvalue is 0, which is the sign for the branch of the limit point. In addition, the second normalization coefficient is $a = -7.303210\text{e}-01$.

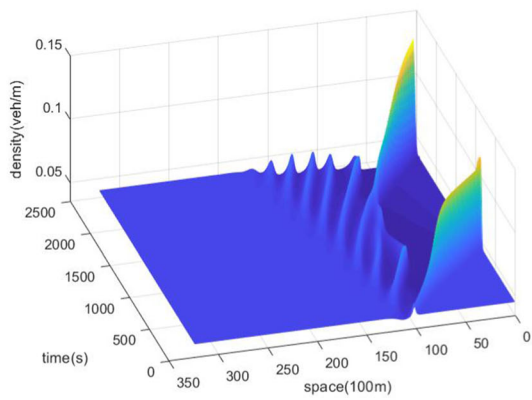
A second limit branch occurs when the variable parameter is 0.172588. The state variables is (0.112377,0), and the corresponding vehicle density is $\rho_0 = 0.112377\text{eh/m}$. The eigenvalues are $-6.0878\text{e}-05$ and 0.038439 , respectively. It is also clear that the first



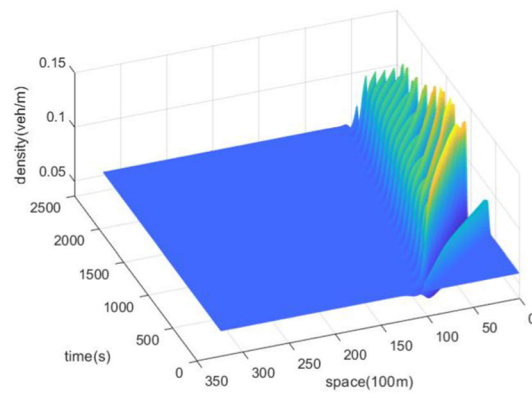
(a) $\rho_0 = 0.01veh/m$



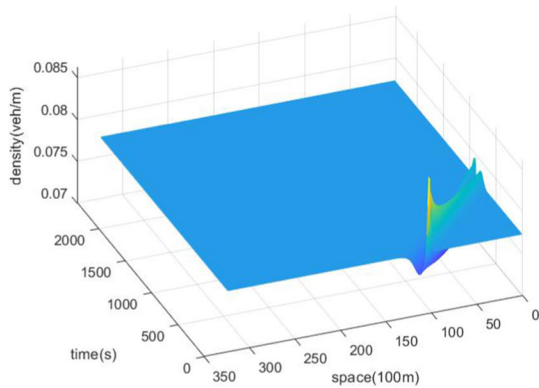
(b) $\rho_0 = 0.03veh/m$



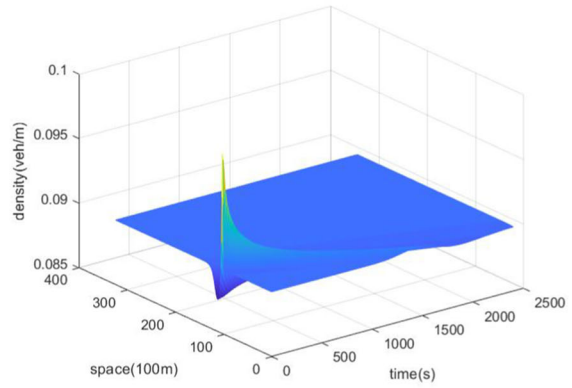
(c) $\rho_0 = 0.04586veh/m$



(d) $\rho_0 = 0.06veh/m$



(e) $\rho_0 = 0.077312veh/m$



(f) $\rho_0 = 0.09veh/m$

Fig. 3 a–f Spatio-temporal graph of density under different initial densities. g–j Under the same density, the FVD model is compared with the space–time diagram considering the density of the throttle model

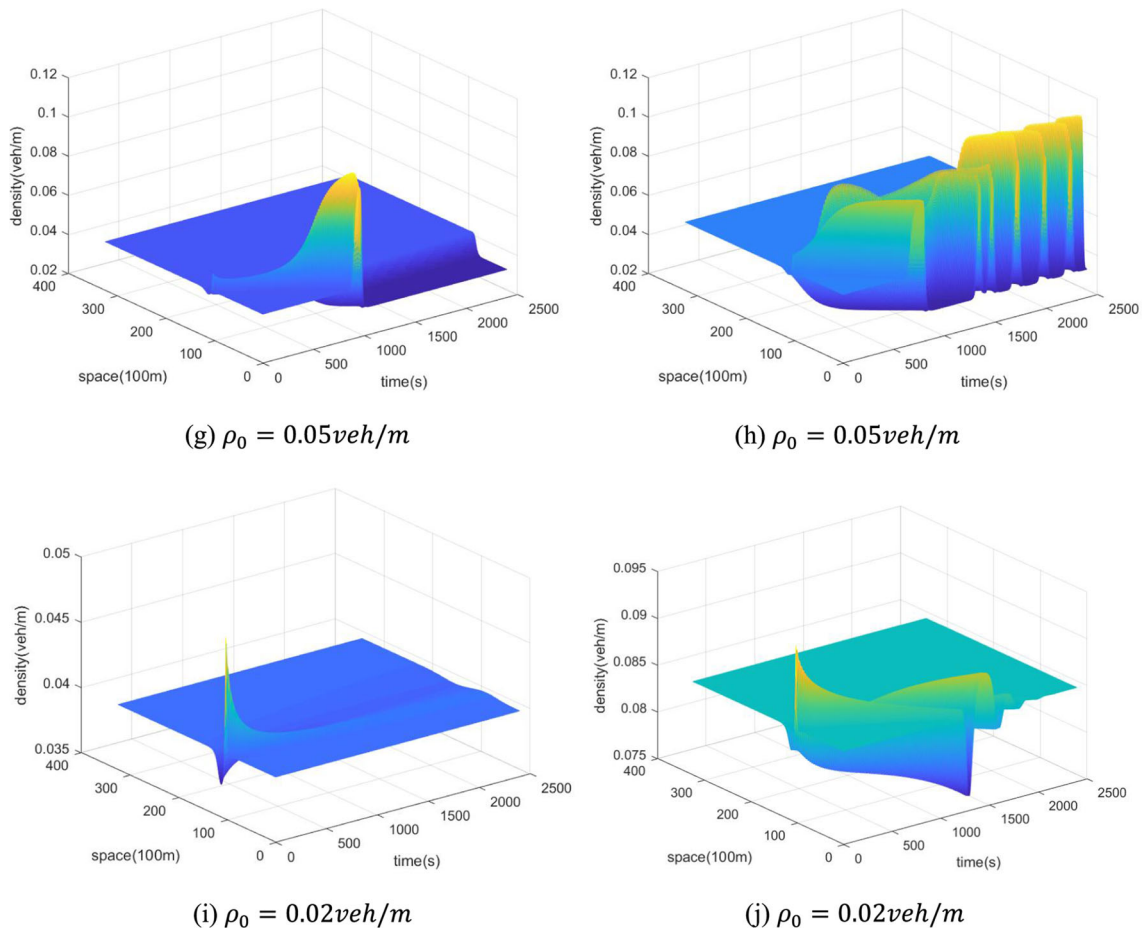


Fig. 3 continued

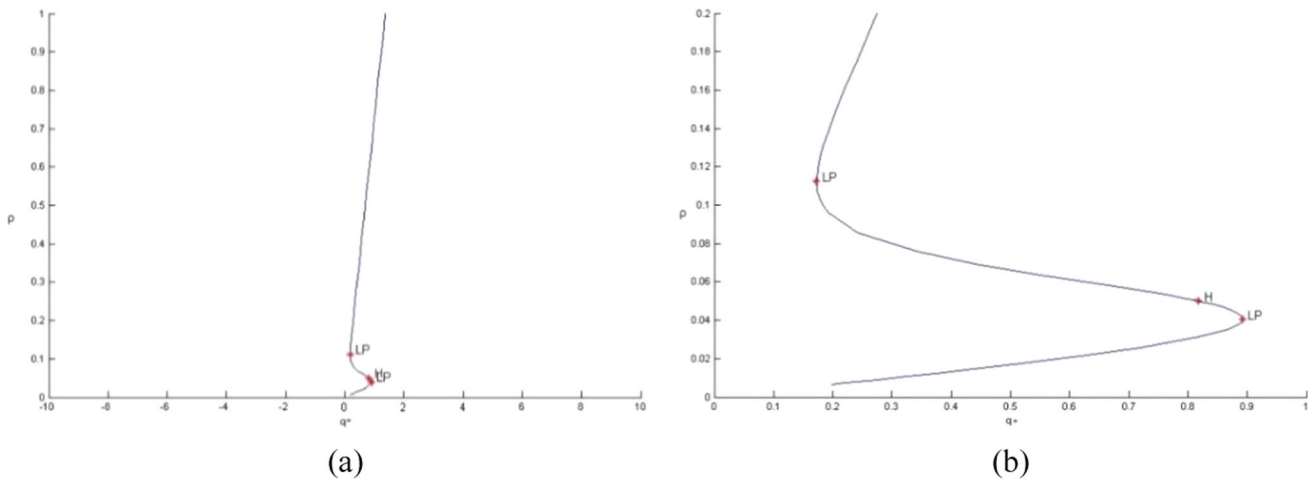


Fig. 4 a The branch diagram where q_* takes the state variable of a large range of parameters as; b Branch graphs with appropriate parameter interval q_*

eigenvalue is 0, which is a sign that it is a branch of the limit point. The second normalization coefficient is $a = 3.502079e-01$.

Below, this paper analyzes the stability changes of the traffic system when the parameters pass some branch critical points calculated above. First, to study the effect of Hopf branch on traffic flow, the stability of the system on the phase plane is investigated in this paper when parameter q_* passes 0.817848.

Figure 5a shows that when the parameter is $q_* < 0.817848$, point $(0.036995, 0)$ is an equilibrium node. Meanwhile, the equilibrium point $(0.044323, 0)$ is a spiral point, and all curves approach the point $(0.044323, 0)$ within the red line. Therefore, the system inside the red line is stable, and the system outside the red line is unstable.

As can be seen from Fig. 5b, when parameter $q_* > 0.817848$, no new equilibrium point appears at Hopf branch point, but periodic solution exists (black region in Figure). This is because in Fig. 5b, when $z \rightarrow +\infty$, one spiral trajectory starts from the point $(0.030112, 0)$ and approaches the focus $(0.051189, 0)$, and eventually evolves into constant amplitude oscillation as $z \rightarrow -\infty$, while the other spiral trajectory approaches the periphery of the constant amplitude oscillation region as $z \rightarrow -\infty$ and approaches infinity as $z \rightarrow +\infty$. So there's a limit cycle between the blue and black lines. These theoretical analyses are also consistent with the above numerical results.

By selecting some branch points as the initial average density of density time evolution, it is helpful for us to better understand the complex phenomena in congested traffic. We analyze the application of local perturbation under the condition of initial uniform density. The initial density is shown below [47].

$$\rho(x, 0) = \rho_0 + \Delta\rho_0 \left\{ \cosh^{-2} \left[\frac{160}{L} \left(x - \frac{5L}{16} \right) \right] - \frac{1}{4} \cosh^{-2} \left[\frac{40}{L} \left(x - \frac{11L}{32} \right) \right] \right\} \quad (78)$$

$$v(x, 0) = V(\rho(x, 0))x \in [0, L] \quad (79)$$

where ρ_0 is the initial density, $\Delta\rho_0 = 0.01\text{veh/m}$ is the disturbance density, $L = 32.2\text{km}$ is the section length, and the dynamic near boundary condition is given by the following formula:

$$\begin{aligned} \rho(1, t) &= \rho(2, t), \rho(L, t) = \rho(L - 1, t), v(1, t) \\ &= v(2, t), v(L, t) = v(L - 1, t) \end{aligned} \quad (80)$$

To facilitate simulation implementation, the space spacing is equal to 100 m, and the time interval is 1 s. The values of other parameters in the model are as follows: $T = 10\text{s}$, $c_0 = 11\frac{\text{m}}{\text{s}}$, $\mu = 550$, $v_f = \frac{30\text{m}}{\text{s}}$, $\rho_m = 0.2\text{veh/m}$.

The state variable $\rho_0 = 0.050047\text{veh/m}$ corresponding to Hopf branch point is selected as the initial uniform density value, and a local small disturbance with

amplitude $\Delta\rho_0 = 0.01\text{veh/m}$ is applied to draw the density space–time diagram of the system, as shown in Fig. 6:

We know from the property of Hopf branching that the system generates a periodic solution from the equilibrium point when the parameter passes through the branching point. Since the initial density value at this time is within the unstable range of the model, the small disturbance on the initial uniform density is amplified, as shown in Fig. 6, and then evolves into periodic oscillation of constant amplitude, which is consistent with the characteristics of the limit cycle solution, indicating that under the initial uniform traffic condition, when the parameter passes Hopf branch point, the small disturbance will change into walking and stopping wave. It is also shown that the results are in agreement with the actual phenomenon and the numerical results, which verifies the correctness of the theoretical analysis.

Next, this paper studies the effect of limit cycle branch on traffic flow when parameter q_* passes 0.891695. When the traffic system passes through the first LP bifurcating point with parameter 0.891695, the stability of the traffic flow will change significantly. First, consider $q_* < 0.891695$. At this point, we set $q_* = 0.79$, the system has two point, one is a saddle point $(0.029518, 0)$, the other is a spiral point $(0.051791, 0)$, as shown in Fig. 7a. All curve within the red line point to point $(0.051791, 0)$. Therefore, the traffic system inside the Red Line is stable, while the traffic system outside the Red line is unstable. With the increase of the parameter, the two equilibrium points gradually move towards the middle. When the parameter is $q_* = 0.891695$, the two equilibrium points shown in Fig. 7a merge into one equilibrium point and a saddle knot branch occurs, as shown in Fig. 7b. Again, the traffic system inside the Red Line is stable, while the traffic system outside the Red line is unstable. With the continuous increase of parameter value, when parameter $q_* > 0.891695$, the equilibrium point disappears, as shown in Fig. 7c, and the whole traffic system becomes unstable.

According to the Hartman-Grossman linearization theorem, when the real part (29) of the eigenvalue of the equation is non-zero, the stability of the equilibrium point of the nonlinear system (26) can be approximated by the saturation of the corresponding linearized system (27). When the equilibrium point is not the central point, the two systems are uniformly stable or uniformly unstable at these equilibrium points. We can solve the equilibrium point of Eq. (26). The optimal speed function in the model is specified as follows:

$$V_e(\rho) = v_f \left\{ \left[1 + \exp \left(\frac{\rho/\rho_m - 0.25}{0.06} \right) \right]^{-1} - 3.72 \times 10^{-6} \right\} \quad (81)$$

In the original model:

$$V_e \left(\frac{\rho(x, t)}{1 + \delta} \right)$$

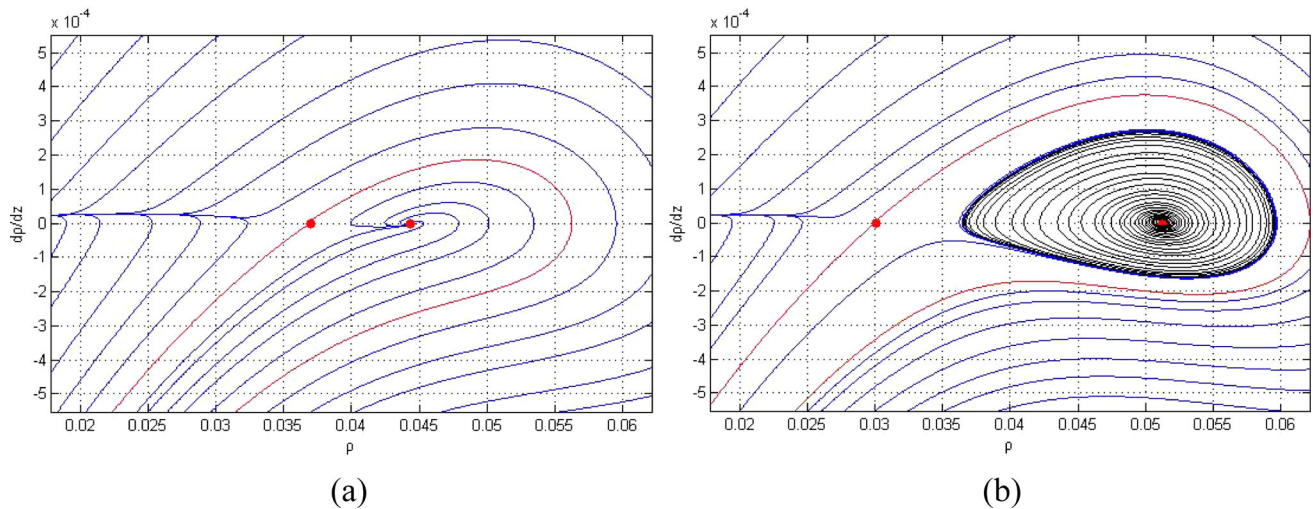
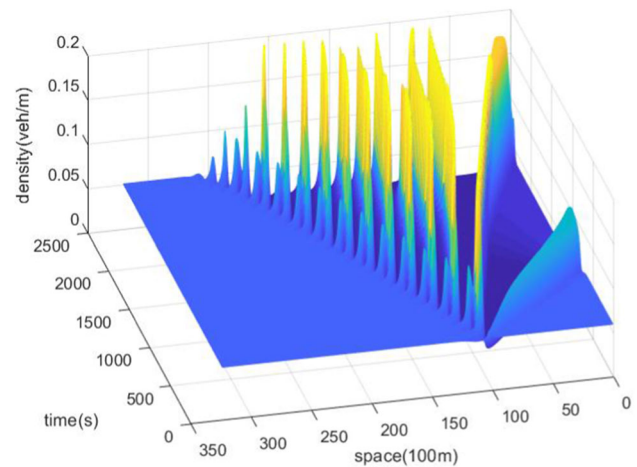


Fig. 5 Phase planar graph of Hopf branch with parameter $q_* < 0.817848$ and parameter $q_* > 0.817848$ **a** phase planar graph with variable parameter $q_* = 0.80$; **b** phase plan for variable parameter $q_* = 0.88$

Fig. 6 The space–time diagram of density with Hopf branch as the initial value



$$= v_f \left\{ \left[1 + \exp\left(\frac{\rho/(1 + \delta)\rho_m - 0.25}{0.06}\right) \right]^{-1} - 3.72 \times 10^{-6} \right\} \tag{82}$$

v_f represents the free flow velocity and ρ_m represents the maximum crowding density.

This may help improve our understanding of complex phenomena in heavy traffic by selecting some branch points as the initial average density of the time evolution of density. We analyze the application of local perturbation under the condition of initial uniform density. The initial density is used as follows [47]:

$$\rho(x, 0) = \rho_0 + \Delta\rho_0 \left\{ \cosh^{-2} \left[\frac{160}{L} \left(x - \frac{5L}{16} \right) \right] - \frac{1}{4} \cosh^{-2} \left[\frac{40}{L} \left(x - \frac{11L}{32} \right) \right] \right\} x \in [0, L] \tag{83}$$

$$v(x, 0) = V(\rho(x, 0)), x \in [0, L] \tag{84}$$

where ρ_0 is the initial mean density, $\Delta\rho_0$ is the amplitude of the local disturbance, and $L = 32.2\text{km}$ is the length of the considered section. The dynamic approximate boundary conditions are given by Eq. (84).

For calculation purposes, the space domain is divided into equal intervals of 100 m in length, and the time interval is selected as 1 s. Relevant parameters of this model are as follows:

$$\begin{aligned} \Delta &= 5\text{m}, c_0 = 11\text{m/s}, p = 0.2, v_f \\ &= 30\text{m/s}, \rho_m = 0.2\text{veh/m}, \delta = 0.5 \end{aligned}$$

When parameter q_* passes LP bifurcating point 0.891695, Vehicle density $\rho_0 = 0.040668$, saddle junction bifurcating occurs. From the above data, it can be seen that before and after the vehicle density passes the saddle junction branch, the fluctuation range of traffic flow density becomes significantly larger, which indicates that when the system passes the saddle junction branch, the traffic flow system changes from a stable state to an unstable state, as shown in Fig. 8.

Secondly, when parameter q_* passes through another LP branch point 0.172588, the stability of traffic flow

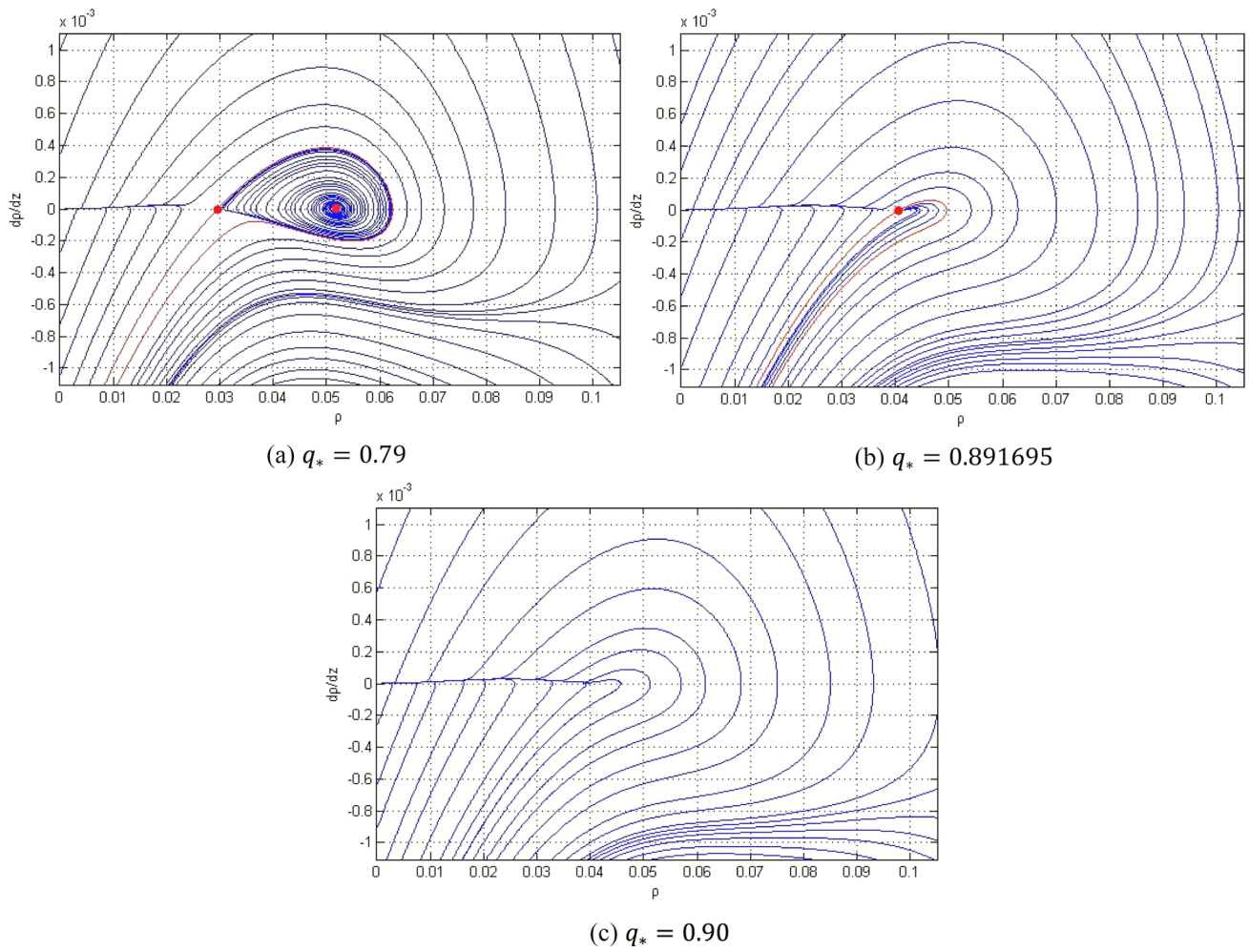


Fig. 7 Phase plan of saddle junction branch when variable parameters $q_* > 0.891695$, $q_* = 0.891695$ and $q_* < 0.891695$ change from small to large

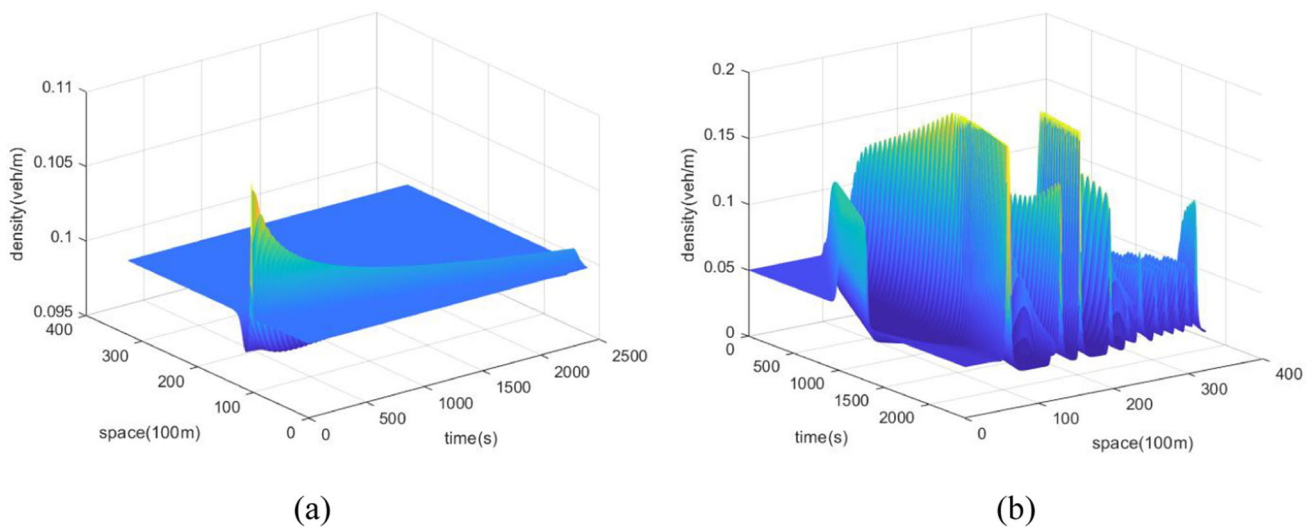


Fig. 8 Density fluctuation state near saddle junction branch under different initial densities. **a** $\rho_0 = 0.040225$ veh/m, **b** $\rho_0 = 0.041231$ veh/m

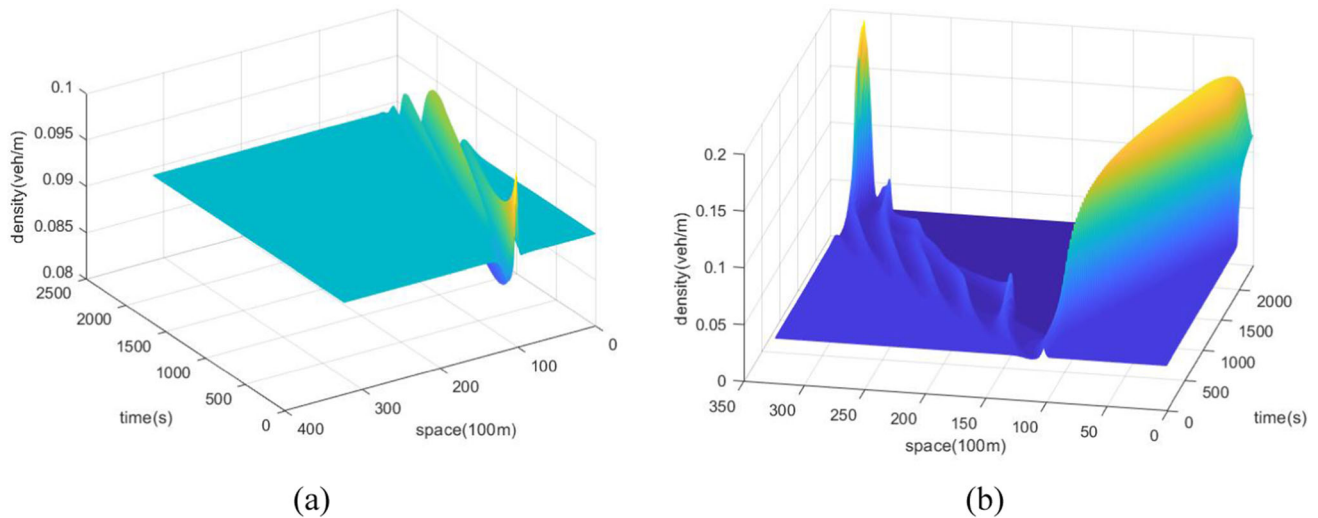


Fig. 10 Density fluctuation state near saddle junction branch under different initial densities. **a** $\rho_0 = 0.104885 \text{ veh/m}$ **b** $\rho_0 = 0.12448531 \text{ veh/m}$

paper, the throttle dynamics information of automobile dynamics is studied at the macroscopic traffic level. Firstly, a macro-traffic flow model considering throttle dynamics information is proposed, and the effectiveness of the model is analyzed. Secondly, in view of the proposed macro model, the stability analysis of the proposed macro-traffic flow model is carried out using the small perturbation method, and the branch analysis method is used to discuss the type and stability of the equilibrium solution, and prove the existence conditions of hopf branch and saddle node branch, and the stability changes of the system when it passes through the branch point are analyzed by numerical simulation. Finally, it is concluded from the spatio-temporal diagram of the system density that the new model has a good effect on stability, elimination of external disturbance and anti-interference ability, which further verifies the validity of the proposed continuous model and it is consistent with the theoretical analysis results. However, vehicles in the actual complex traffic system are affected by a variety of dynamic information, such as wind resistance, tire side longitudinal force and other dynamic information, which also are some directions that need to be further understood in the future.

Acknowledgements The authors would like to thank the anonymous referees and the editor for their valuable opinions. This work is partially supported by the National Natural Science Foundation of China under the Grant Nos. (61863032, 11965019) and the China Postdoctoral Science Foundation Funded Project (Project No.: 2018M633653XB) and the Natural Science Foundation of Gansu Province of China under the Grant No. 20JR5RA533 and the Qizhi Personnel Training Support Project of Lanzhou Institute of Technology (2018QZ-11) and Gansu Province Educational Research Project (Grant No. 2021A-166).

Author contributions

WHA: Participate in research: propose research topics; Design research scheme; Implement the research process; Final paper. MMW: Article writing: research and collate literature; Design the paper framework; Draft a paper; Revise the thesis; Organize data. DWL: Work support: statistical analysis; Access to research funding; Technical or material support; Instructional support.

Data availability The manuscript has associated data in a data repository [Authors' comment: In this paper, based on the macroscopic traffic flow model considering throttle dynamics, the equilibrium point and its type of the model are studied by bifurcation analysis method, and the conclusion that the theory is consistent with the simulation is obtained. However, there are many factors that affect the traffic state, which is also the direction of our later research].

Declarations

Conflict of interest The authors declared that they have no conflicts of interest to this work. We declare that we do not have any commercial or associative interest that represents a conflict of interest in connection with the work submitted.

References

1. J.J. Zhang, Y.P. Wang, G.Q. Lu, Impact of heterogeneity of car-following behavior on a rear-end crash risk. *Accident Anal. Prev.* **125**, 275–289 (2019)
2. Z.H. Yao, T.R. Xu, Y.S. Jiang, R. Hu, Linear stability analysis of heterogeneous traffic flow considering degradations of connected automated vehicles and reaction time. *Phys. A Stat. Mech. Appl.* **561**, 125218 (2021)

3. Y.F. Jin, J.W. Meng, Dynamical analysis of an optimal velocity model with time-delayed feedback control. *Commun. Nonlinear Sci. Numer. Simul.* **90**, 105333 (2020)
4. X. Wang, R. Jiang, L. Li, Y.L. Lin, F.Y. Wang, Long memory is important: a test study on deep-learning based car-following model. *Phys. A Stat. Mech. Appl.* **514**, 786–795 (2019)
5. J. Cattin, L. Leclercq, F. Pereyron, F.E. Faouzi, Calibration of gipps' car-following model for trucks and the impacts on fuel consumption estimation. *IET Intell. Transp. Syst.* **13**, 367–375 (2019)
6. Y.Q. Sun, H.X. Ge, R.J. Cheng, An extended car-following model under V2V communication environment and its delayed-feedback control. *Phys. A Stat. Mech. Appl.* **508**, 349–358 (2018)
7. M.J. Lighthill, G.B. Whitham, On kinematic waves. I. Flood movement in long rivers. *Proc. Math. Phys. Eng. Sci.* **229**, 281–316 (1995)
8. H.Y. Lu, G.H. Song, L. Yu, The acceleration cliff: an investigation of the possible error source of the VSP distributions generated by Wiedemann car-following model. *Transp. Res. D.* **65**, 161–177 (2018)
9. X.Y. Wang, Y.Q. Liu, J.Q. Wang, J.L. Zhang, Study on influencing factors selection of driver's propensity. *Phys. A Stat. Mech. Appl.* **66**, 35–48 (2019)
10. Z.P. Li, Q.Q. Qin, W.Z. Li, S.Z. Xu, Y.Q. Qian, J. Sun, Stabilization analysis and modified KdV equation of a car-following model with consideration of self-stabilizing control in historical traffic data. *Nonlinear Dyn.* **91**, 1113–1125 (2018)
11. Y.Y. Qin, H. Wang, Analytical framework of string stability of connected and autonomous platoons with electronic throttle angle feedback. *Transportmetrica A* **17**, 59–80 (2021)
12. T.Q. Tang, Z.Y. Yi, J. Zhang, T. Wang, J.Q. Leng, A speed guidance strategy for multiple signalized intersections based on car-following model. *Phys. A Stat. Mech. Appl.* **496**, 399–409 (2018)
13. P. Zhang, Y. Xue, Y.C. Zhang, X. Wang, B.L. Cen, A macroscopic traffic flow model considering the velocity difference between adjacent vehicles on uphill and downhill slopes. *Mod. Phys. Lett. B* **34**, 2050217 (2020)
14. T.Q. Tang, W.F. Shi, H.J. Huang, W.X. Wu, Z.Q. Song, A route-based traffic flow model accounting for interruption factors. *Phys. A Stat. Mech. Appl.* **514**, 767–785 (2019)
15. X. Wu, X.M. Zhao, H.S. Song, Q. Xin, S.W. Yu, Effects of the prevision relative velocity on traffic dynamics in the ACC strategy. *Phys. A Stat. Mech. Appl.* **515**, 510–517 (2019)
16. D. Kawecki, B. Nowack, A proxy-based approach to predict spatially resolved emissions of macro- and microplastic to the environment. *Sci. Total Environ.* **748**, 141137 (2020)
17. Q.Y. Wang, H.X. Ge, An improved lattice hydrodynamic model accounting for the effect of backward looking and flow integral. *Phys. A Stat. Mech. Appl.* **513**, 438–446 (2019)
18. C.T. Jiang, R.J. Cheng, H.X. Ge, An improved lattice hydrodynamic model considering the backward looking effect and the traffic interruption probability. *Nonlinear Dyn.* **91**, 777–784 (2018)
19. C.X. Ma, R.C. He, W. Zhang, Path optimization of taxi carpooling. *PLoS ONE* **13**(8), e0203221 (2018)
20. C. Samaras, D. Tsokolis, S. Toffolo, G. Magra, L. Ntziachristos, Z. Samaras, Improving fuel consumption and CO₂ emissions calculations in urban area by coupling a dynamic micro traffic model with an instantaneous emissions model. *Trans. Res. D* **65**, 772–783 (2018)
21. D. Guo, J. Wang, J.B. Zhao, A vehicle path planning method based on a dynamic traffic network that considers fuel consumption and emissions. *Sci. Total Environ.* **663**, 935–943 (2019)
22. T.Q. Tang, Z.Y. Yi, Q.F. Lin, Effects of signal light on the fuel consumption and emissions under car-following model. *Phys. A Stat. Mech. Appl.* **469**, 200–205 (2017)
23. Y. Igarashi, Quasi-solitons in dissipative systems and exactly solvable lattice models. *J. Phys. Soc. Jpn.* **68**, 791–796 (1999)
24. M. Bando, K. Hasebe, A. Shibata, Y. Sugiyama, Dynamical model of traffic congestion and numerical simulation. *Phys. Rev. E* **51**, 1035–1042 (1995)
25. Y.F. Jin, M. Xu, Bifurcation analysis of the full velocity difference model. *Chin. Phys. Lett.* **27**(4), 040501 (2010)
26. W. Ai, Z. Shi, D. Liu, Bifurcation analysis method of nonlinear traffic phenomena. *Int. J. Mod. Phys. C* **26**, 1550111 (2015)
27. Yu. Yicai Zhang, P.Z. Xue, D. Fan, H. di He, Bifurcation analysis of traffic flow through an improved car-following model considering the time-delayed velocity difference. *Physica A* **514**, 133–140 (2019)
28. W. Ren, R. Cheng, H. Ge, Bifurcation analysis of a heterogeneous continuum traffic flow model. *Appl. Math. Model.* **94**, 369–387 (2021)
29. P. Richards, Shock waves on the highway. *Oper. Res.* **4**(1), 42–51 (1956)
30. R. Delpiano, J. Laval, J. Coeymans et al., The kinematic wave model with finite decelerations: a social force car-following model approximation. *Transp. Res. B Methodol.* **71**, 182–193 (2015)
31. R. Jiang, Q. Wu, Z. Zhu, Full velocity difference model for a car-following theory. *Phys. Rev. E* **64**(1), 017101–017105 (2001)
32. Y. Li, L. Zhang, S. Peeta et al., A car-following model considering the effect of electronic throttle opening angle under connected environment. *Nonlinear Dyn.* **85**(4), 1–11 (2016)
33. X.P. Meng, L.Y. Yan, Stability analysis in a curved road traffic flow model based on control theory. *Asian J. Control.* **19**, 1844–1853 (2017)
34. Z.Z. Liu, H.X. Ge, R.J. Cheng, KdV-Burgers equation in the modified continuum model considering the effect of friction and radius on a curved road. *Phys. A Stat. Mech. Appl.* **503**, 1218–1227 (2018)
35. R. Kaur, S. Sharma, Modeling and simulation of driver's anticipation effect in a two-lane system on curved road with slope. *Phys. A Stat. Mech. Appl.* **499**, 110–120 (2018)
36. J. Hedrick, D. McMahon, V. Narendran et al., Longitudinal Vehicle Controller Design for IVHS Systems. In *American Control Conference (IEEE, 1991)*, pp. 3107–3112.
37. K. Li, P. Ioannou, Modeling of traffic flow of automated vehicles. *IEEE Trans. Intell. Transp. Syst.* **5**(2), 99–113 (2004)

38. P. Ioannou, Z. Xu, Throttle and brake control systems for automatic vehicle following. *Inst. Transport. Stud. UC Berkeley* **1**(4), 345–377 (1994)
39. S. Jin, D. Wang, P. Tao et al., Non-lane-based full velocity difference car following model. *Physica A* **389**(21), 4654–4662 (2010)
40. Y. Xue, L. Dong, Y. Yuan et al., Numerical simulation on traffic flow with the consideration of relative velocity. *Acta Phys. Sin.* **51**(3), 495–496 (2002)
41. Y. Xue, A car-following model with stochastically considering the relative velocity in a traffic flow. *Acta Phys. Sin.* **52**(11), 2750–2756 (2003)
42. H. Gong, H. Liu, B. Wang, An asymmetric full velocity difference car-following model. *Physica A* **387**(11), 2595–2602 (2008)
43. H. Ge, R. Cheng, Z. Li, Two velocity difference model for a car following theory. *Physica A* **387**(21), 5239–5245 (2008)
44. B.S. Kerner, P. Konhäuser, Cluster effect in initially homogeneous traffic flow. *Phys. Rev. E* **48**, 2335–2338 (1993)
45. J.F. Cao, C.Z. Han, Y.W. Fang, *Nonlinear Systems Theory and Application* (Xi'an Jiao Tong University Press, Xi'an, 2006)
46. Y.A. Kuznetsov, *Elements of Applied Bifurcation Theory* (Springer, New York, 1998), pp.151–194
47. R. Jiang, Q.S. Wu, Z.J. Zhu, A new continuum model for traffic flow and numerical tests. *Transport. Res. B Methodol.* **36**, 405–419 (2002)

Springer Nature or its licensor (e.g. a society or other partner) holds exclusive rights to this article under a publishing agreement with the author(s) or other rightsholder(s); author self-archiving of the accepted manuscript version of this article is solely governed by the terms of such publishing agreement and applicable law.